Analysis of Surface Fluxes in the Marine Atmospheric Boundary Layer in the Vicinity of Rapidly Intensifying Cyclones

GENNARO H. CRESCENTI* AND ROBERT A. WELLER

Woods Hole Oceanographic Institution, Woods Hole, Massachusetts

(Manuscript received 18 April 1991, in final form 23 September 1991)

ABSTRACT

A mooring with a surface buoy was deployed about 300 km southeast of Nova Scotia during the Experiment on Rapidly Intensifying Cyclones over the Atlantic (ERICA) in an attempt to obtain long-term, high-quality measurements of meteorological and near-surface oceanographic data. The acquired surface data included sea surface temperature, air temperature, relative humidity, barometric pressure, wind velocity, incident solar radiation, and downward longwave radiation. A limited time series of sea temperature and current velocity was gathered from current meters at 20 and 50 m beneath the sea surface.

The surface meteorology was described before, during, and after the passage of three rapidly intensifying cyclones. Estimates of the surface air–sea heat fluxes, computed from bulk aerodynamic formulas, were also examined for these same storms. A simple heat budget was used to estimate the heat loss or gain of the upper ocean against the air–sea heat transfer at the ocean surface. While the total surface heat flux may sometimes exceed 1000 W m^{-2}, the data suggest that the main mechanism for cooling the upper-ocean water was principally advective. An examination of the air–sea momentum transfer shows that the atmosphere exerted a significant influence on the upper ocean; persistent westerly winds coming off the North American continent transported surface waters to the south.

1. Introduction

As part of the Experiment on Rapidly Intensifying Cyclones over the Atlantic (ERICA), a surface mooring was deployed in the North Atlantic Ocean approximately 300 km southeast of Halifax, Nova Scotia. This mooring collected a 140-day time series of near-surface meteorology and upper-ocean variability. The objective of our participation in the cooperative field experiment was to examine and describe the mean surface meteorology, the surface fluxes of heat, moisture, and momentum in the ERICA region before, during, and after the passage of rapidly intensifying cyclones. ERICA was part of the Office of Naval Research's (ONR) Heavy Weather at Sea program. The principal objectives of the experiment were to understand fundamental physical processes occurring in the atmosphere during rapid intensification of winter cyclones at sea, to determine those physical processes that need to be incorporated into dynamical prediction models through efficient parameterizations, and to identify measurable precursors that must be incorporated into initial analysis for accurate and detailed operational model predictions (Hadlock and Kreitzberg 1988).

Rapidly intensifying cyclones or "bombs" frequent the western North Atlantic Ocean from Cape Hatteras northeast to the Grand Banks of Newfoundland (Hadlock and Kreitzberg 1988). A bomb is defined as a storm whose central surface pressure drops at least 1 mb h^{-1} for 24 h at 60°N (Sanders and Gyakum 1980). These storms usually occur in and around areas of large sea surface temperature gradients (i.e., the Gulf Stream). Bombs often exhibit hurricane-like features in the wind and cloud fields and can be disruptive and destructive to maritime activities and coastal communities. An example of this destructive potential was seen during ERICA when winds on the northwest side of an intense storm capsized the deep-sea drilling rig *Rowan Gorilla I.* The incident occurred while the rig was being towed away from the Nova Scotia offshore oil fields (Marine Weather Review 1989). The rig sank several days later. In addition, 27 crewmen were forced to abandon the rig and spent nearly 24 hours in a survival capsule before being rescued.

Many of the physical processes that contribute to the development and rapid intensification of these storms are still not fully understood. Although it is likely that baroclinic processes are the single most important factor in explosive developments (Davis and Emanuel 1988), the debate continues on the relative

* Current affiliation: North Carolina State University, Raleigh, North Carolina.

Corresponding author address: Gennaro H. Crescenti, Department of Marine, Earth and Atmospheric Sciences, Box 8208, North Carolina State University, Raleigh, NC 27695-8208.

contributions of jet streaks, upper-level dynamic forcing, latent heat release throughout the troposphere, static stability, interaction of preexisting disturbances, sea surface temperature distribution, and air–sea interaction.

Air–sea fluxes were recognized long ago (Winston 1955; Pyke 1965) as playing a role in explosive maritime cyclogenesis. However, the exact nature of their contribution to storm development and maintenance has not yet been fully resolved. Some details are beginning to emerge from recent research on the complex role in storm development played by surface transfers of sensible and latent heat (Sanders and Auciello 1989). It is generally thought that the sensible and latent heat fluxes act well in advance to precondition the atmosphere. Boundary-layer instability increases when cold, dry air from Canada flows southward over increasingly warm ocean water and is heated and moistened from below (Reed and Blier 1986b; Wash et al. 1988). The sensible heat flux may indirectly exert a significant influence by reducing the static stability of the large-scale environment, while the moisture flux plays an important role by increasing air buoyancy and providing latent heat that is later released in convective showers (Reed and Blier 1986a; Nuss and Anthes 1987).

In ERICA, a surface mooring was deployed equipped with both meteorological and oceanographic instrumentation. The intent was to provide high-quality in situ observations; to use those observations to document the air–sea fluxes before, during, and after the passage of bombs; and to examine the response of the ocean to the surface forcing associated with the bombs. A description of the mooring and data is given in section 2. The surface meteorology of three bombs is discussed in section 3 followed by analysis of the air–sea surface heat fluxes in section 4 for those same storms. The air–sea momentum transfers are the subject of section 5 and this study is summarized in section 6.

2. ERICA surface mooring

A surface mooring was deployed in the eastern edge of the ERICA storm region at 42°33′N, 61°14′W in 2984 m of water on 17 October 1988. The mooring

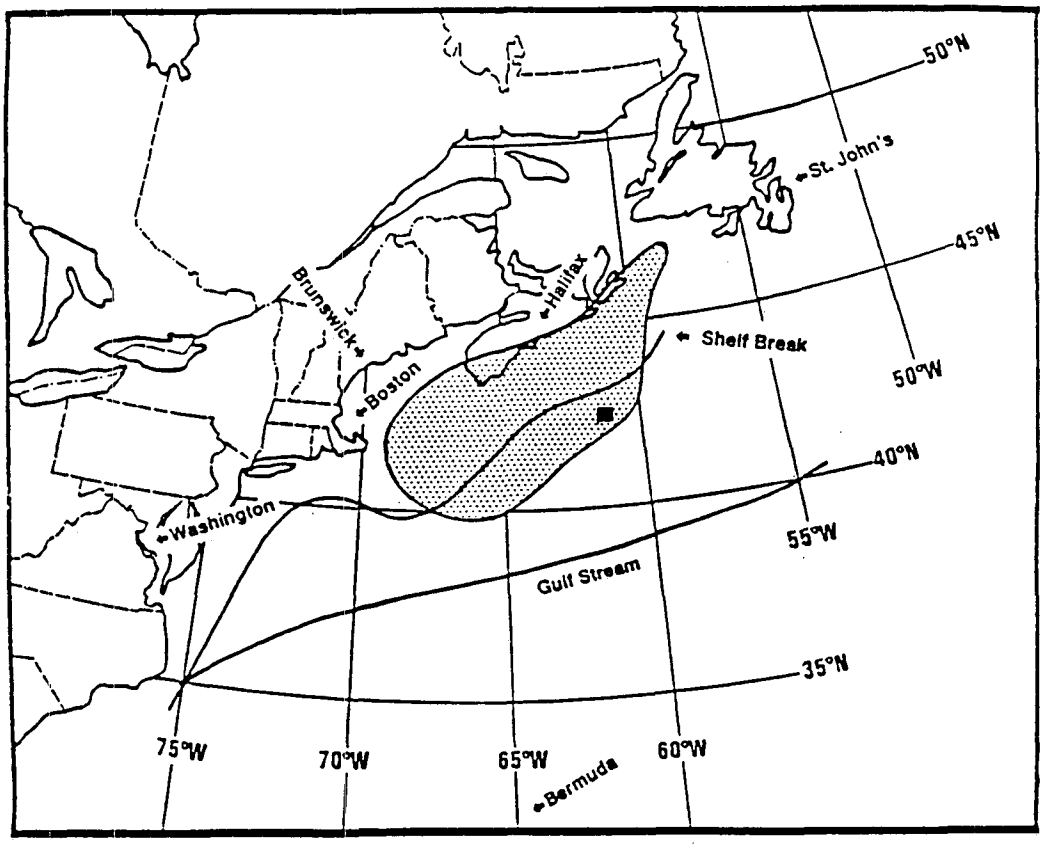

FIG. 1. ERICA mooring location (map from Hadlock and Kreitzberg 1988). The mooring was located at approximately 42°33′N, 61°14′W (black box). The stippling denotes the region in which the largest decreases in surface atmospheric pressure with time are found for ERICA-type storms. The smoothed continental shelf boundary (100 fathoms) and Gulf Stream mean position (to the south) are also shown.

was situated about 300 km southeast of Nova Scotia and north of the Gulf Stream (Fig. 1) at the latitude of maximum bomb occurrence (Roebber 1984). Recovery of the mooring occurred on 7 March 1989 after 140 days at sea. The surface platform was a 3-m-diameter aluminum discus buoy with meteorological sensors placed 3 m above the mean waterline on top of a single mast (Fig. 2). The single mast design was developed to minimize icing of the superstructure. A technical description of the mooring was given by Kery (1989).

Two vector-averaging wind recorders (VAWR) (Weller et al. 1990; Dean and Beardsley 1988; Payne 1974) were placed on the buoy to measure surface meteorology. There were two reasons for having two independent data-acquisition systems. First, in the event that one particular sensor failed, the same sensor on the other VAWR would act as a backup. Second, confidence was gained in sensor reliability by comparing two time series; this also provided an estimation of the uncertainty of each variable. This was extremely important since the harsh marine environment placed great demands on the mooring and its instrumentation. Each VAWR measured

- sea surface temperature (Thermometrics thermistor, located at 0.75 and 1.75 m below the sea surface);
- air temperature (YSI 44034 thermistor);
- relative humidity (Vaisala 1518HM Humicap);
- barometric pressure (Paroscientific 215AW-020 Digiquartz);
- incident solar radiation (Eppley 8-48 black and white pyranometer);
- downward longwave radiation (Eppley PIR pyrgeometer);
- wind speed and direction (R. M. Young 5103 wind monitor on one VAWR; R. M. Young 6101 Gill aluminum three-cup anemometer and WHOI-built glass-reinforced, plastic vane on the other VAWR).

These data were recorded internally on magnetic cassette tapes every 15 min. A time series from one of the VAWRs (designated as V-161WR) is shown in Fig. 3 for the entire deployment. Each VAWR worked well for the duration of the mooring deployment. Meteorological data telemetered via satellite (Argos) were checked on a daily basis for agreement with surface synoptic weather maps and other nearby surface observations. Two months into the deployment on 13 December 1988 the R/V *Dawson* was able to make a visual inspection of the mooring. Observations of sea surface temperature, air temperature, relative humidity, barometric pressure, wind speed, and wind direction made on the *Dawson* were in agreement with the data measured by the VAWR sensors. No evidence of damage to the buoy or sensors was observed. The buoy and sensors were still in good condition when the mooring was recovered in early March 1989. After recovery, the

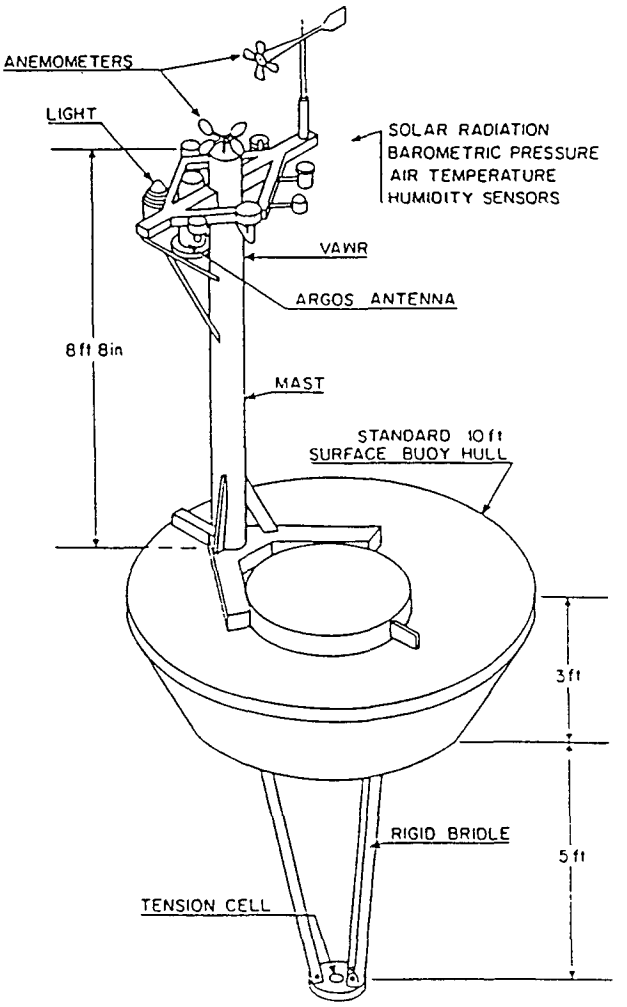

FIG. 2. ERICA buoy.

sensors were calibrated, and the pre- and postdeployment calibrations compared (Crescenti et al. 1991).

Small or negligible change was found in most of the sensor calibrations. Only one sensor failed during the mooring deployment. The calibration of one relative humidity sensor became unstable after the passage of a bomb on 4 January 1989. Although the sensor never ceased to function during the deployment, data values became erratic and unrealistic. Fortunately, the other relative humidity sensor worked well during the experiment and displayed negligible drift. Details of sensor performance were discussed by Crescenti et al. (1991). The mean and standard deviation of each variable is given in Table 1 as well as linear regressions between each pair of variables. Oceanographic data were acquired with two vector-measuring current meters (VMCM) (Weller and Davis 1980) placed on the mooring to measure velocity (east and north components) and water temperature at 20 and 50 m below the sea surface. These data were recorded internally on

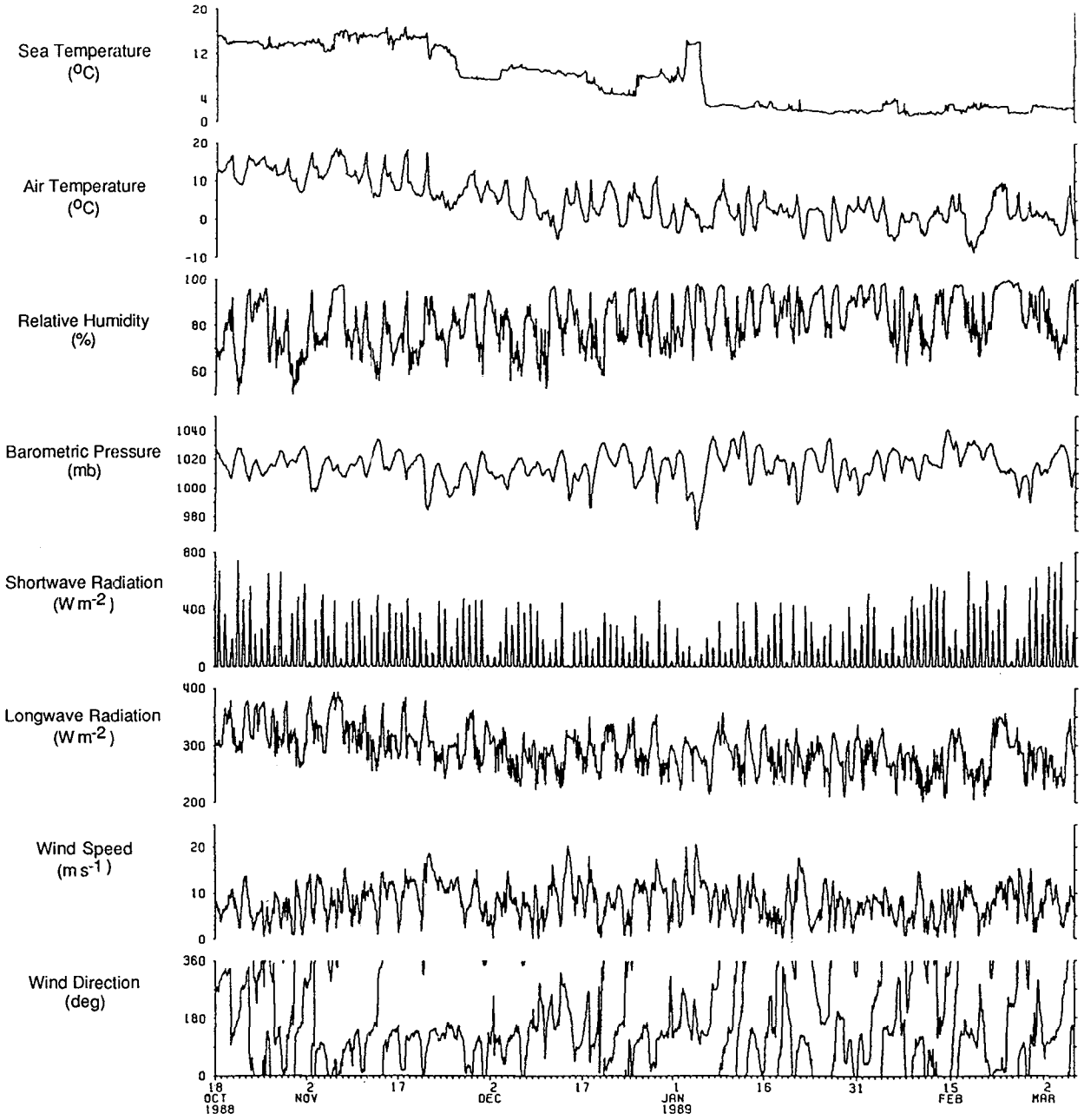

FIG. 3. Complete time series of meteorological data taken from the ERICA mooring from V-161WR. From top to bottom: Sea surface temperature (°C), air temperature (°C), relative humidity (%), barometric pressure (mb), incident solar radiation (W m^{-2}), downward longwave radiation (W m^{-2}), wind speed (m s^{-1}), and wind direction (°). Note that the wind direction is in oceanographic coordinates. The value represents the direction to which the wind is blowing.

magnetic cassette tapes every 7.5 min. Unfortunately, these instruments did not fare as well as their meteorological counterparts. The compass housed inside the 50-m VMCM failed on 21 November 1988 when a small amount of seawater leaked into the instrument. Without the compass as a reference, the current direction could not be determined. In addition, the sea temperature data became unreliable. The velocities on both VMCMs were lost after 26 December 1988. It was learned during mooring recovery that commercial fishing lines had tangled and jammed the propeller sensors used to measure velocity. The sea temperature data from the 20-m VMCM were available and good for the duration of the deployment.

TABLE 1. Mean and standard deviations of variables acquired by the VAWRs (V-161WR and V-707WR) on the ERICA buoy from 18 October 1988 through 6 March 1989. Offset A, slope B, correlation coefficient r, and standard error SE of least-squares fit of V-707WR data as a function of V-161WR.

	V-161WR		V-707WR		V-707WR-V161WR	
	Mean	std dev	Mean	std dev	Mean	std dev
Sea surface temperature (°C)	7.27	5.07	7.25	5.07	−0.02	0.03
Air temperature (°C)	4.71	5.57	4.69	5.57	−0.02	0.06
Relative humidity* (%)	77.8	10.7	71.9	12.4	−0.9	3.1
Barometric pressure (mb)	1015.4	10.3	1015.8	10.4	0.4	0.2
Solar radiation (W m^{-2})	65.1	125.5	64.1	126.0	−1.1	19.3
Longwave radiation (W m^{-2})	293.7	35.9	284.7	36.7	−9.0	12.3
East wind (m s^{-1})	2.94	6.10	2.93	6.10	−0.01	0.38
North wind (m s^{-1})	−1.33	5.96	−0.96	5.84	0.36	0.40
	A	B	r	SE		
Sea surface temperature (°C)	−0.01	0.998	1	0.03		
Air temperature (°C)	−0.02	1.000	.9999	0.06		
Relative humidity* (%)	−15.62	1.126	.9747	2.78		
Barometric pressure (mb)	−2.74	1.003	.9997	0.26		
Solar radiation (W m^{-2})	−1.48	0.995	.9785	31.90		
Longwave radiation (W m^{-2})	1.11	0.966	.9428	12.24		
East wind (m s^{-1})	−0.00	0.998	.9981	0.38		
North wind (m s^{-1})	0.34	0.978	.9979	0.38		

* 18 October–31 December 1988

The accuracy of the sensors used with the VAWR has been thoroughly documented by Weller et al. (1990) for a previous air–sea interaction experiment. The same pre- and postdeployment calibrations were carried out on the ERICA time series yielding estimates of uncertainties comparable to those determined by Weller et al. The accuracy of the sea surface temperature was estimated at 0.1°C while the accuracy of the air temperature is less than 0.4°C for wind speeds greater than 3 m s^{-1}. The uncertainty in air temperature quickly increases to 1°–3°C during episodes of low wind and strong solar heating; however, those periods are very short in the ERICA time series. The accuracy of the relative humidity was 5%. The barometric pressure estimates have improved with an uncertainty of about 0.4 mb. The incident solar and downward longwave radiation accuracies were both estimated at 5%. The wind direction was certain to within 3° while more recent calibrations of the wind speeds have uncertainties down to about 2%.

3. Surface meteorology of ERICA storms

The ERICA field study was conducted from 1 December 1988 to 28 February 1989. During this time, eight intensive observation periods (IOPs) were initiated to study rapidly intensifying cyclones in great detail using a vast observation network. A summary of the field experiment and its many observing platforms was discussed by Hadlock and Kreitzberg (1988). As expected, several of these storms passed close to the mooring. The observations made at the buoy provide detailed information about each storm and the storm climatology in the marine atmospheric surface layer. Three case studies were examined, including one storm whose center came within 100 km of the buoy. The beginning and ending dates and times for these three IOPs are given in Table 2. The meteorology observed in each of these storms is described next.

a. IOP 2

This storm contained numerous, complex mesoscale features and was considered one of the best cases of rapid depending seen during the ERICA field study. Cold air was driven southward behind a preceding cold front beyond the north wall of the Gulf Stream. A complex series of upper-level troughs helped initiate several surface lows off the coast of the Carolinas (Hartnett et al. 1989). Eventually, one single low pressure system formed and moved past the buoy to its south and east (Fig. 4a). A barometric pressure drop of approximately 35 mb in 30 h was observed at the buoy from 1200 UTC 13 December to 1800 UTC 14 December (Fig. 5) as the storm came within 450 km

TABLE 2. Beginning and ending dates and times of IOPs 2, 3, and 4 (from Hartnett et al. 1989).

	Start		End	
IOP 2	1500 UTC	12 December 1988	0000 UTC	15 December 1988
IOP 3	0000 UTC	17 December 1988	0000 UTC	19 December 1988
IOP 4	1200 UTC	3 January 1989	1200 UTC	5 January 1989

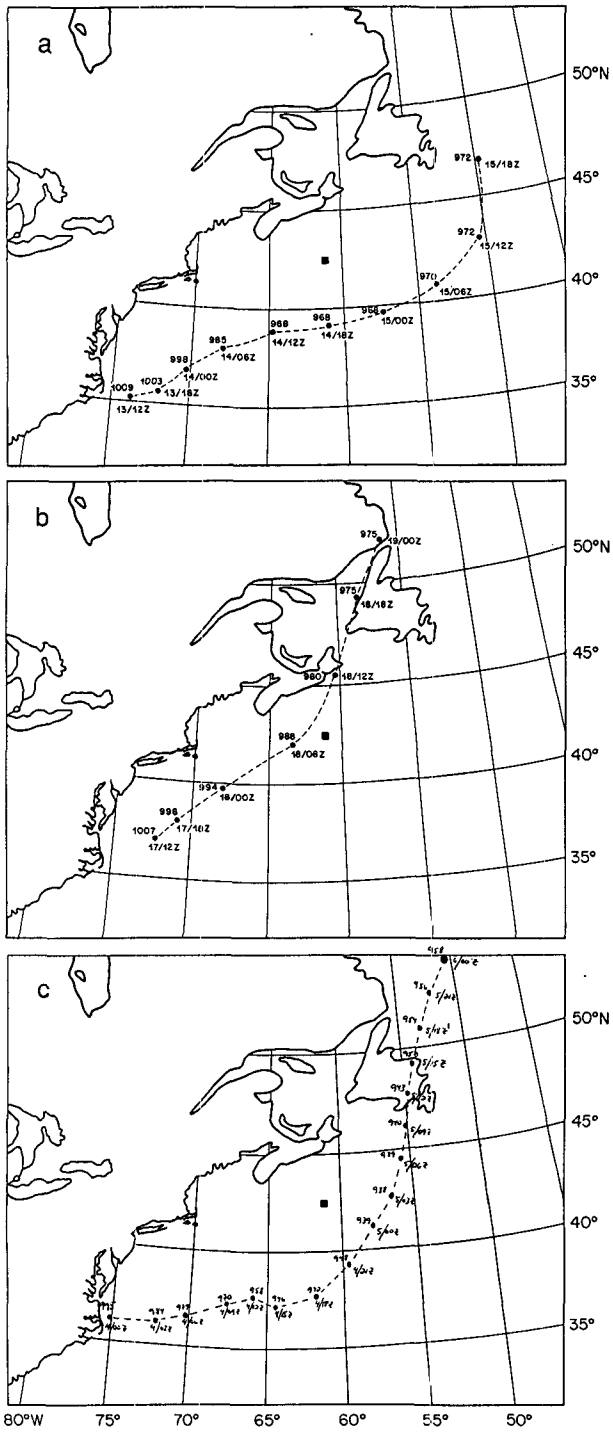

FIG. 4. Storm tracks relative to the ERICA mooring for (a) IOP 2, (b) IOP 3, and (c) IOP 4. These tracks are based on preliminary analyses in Hartnett et al. (1989). Cyclone center barometric pressure (mb) is given with the date and time (UTC).

of the buoy. The minimum observed pressure at the buoy was 990 mb at 1800 UTC 14 December. The pressure gradient between the buoy and the storm center was estimated at 5 mb (100 km)$^{-1}$ for this same time.

The sea surface temperature exhibited little variability and remained between 8° and 9°C before and after the storm. The relative humidity was generally between 80% and saturation during most of the stormy weather. The air temperature was cold at the start of IOP 2 at −2°C. It increased during the next 36 h up to about 8°C as winds from the north veered and blew from the east. During the last 12 h of IOP 2, cold air was swept into the area again as the winds reversed and came from the north. As the storm intensified and approached the buoy, the wind speed increased steadily over a 24-h period up to sustained values of 20 m s^{-1} near the end of IOP 2. The observed solar irradiance was low during 14 December. The solar noon value never exceeded 20 W m^{-2}, indicating very thick cloud cover during the daytime hours. This observation was supported by Geostationary Operational Environmental Satellite (GOES) imagery (Hartnett and Browne 1989). The increase in the observed values of the downward longwave radiation also indicated the approach of the storm as lower and warmer clouds moved into the area. Prior to the storm typical values were about 240 W m^{-2}, which was equivalent to a sky temperature of approximately −18°C. During the storm, the downward longwave flux was about 320 W m^{-2}, or the equivalent of about 1°C.

b. IOP 3

This storm was like IOP 2 in many respects, with several discrete surface centers and complex upper-level forcing. In this case, however, the storm track remained closer to the North American coastline (Fig. 4b). The storm originated off the North Carolina coast and initially moved eastward along a warm front. It eventually gave way to upper-level forcing that steered the surface cyclone northward into a region of cold-air advection between Nova Scotia and Newfoundland (Hartnett et al. 1989). The barometric pressure at the buoy dropped 32 mb in 16 h from midday on 17 December to early on 18 December (Fig. 6). The minimum observed pressure at the buoy was 984 mb at 0500 UTC 18 December when the storm passed less than 100 km to the west of the mooring.

As the storm approached from the southwest, the winds steadily veered and increased to nearly 20 m s^{-1} from the west at 0000 UTC 17 December to the opposite direction at 0500 UTC 18 December. During this same period, the sea surface temperature had a quick steplike drop of 2°C, from 9° to 7°C. The shifting winds replaced the cold, dry air with warmer, moist air as the air temperature increased from 0° to 10°C and the relative humidity increased from 70% to 95%. The downward longwave radiation increased from 280 to about 350 W m^{-2}. This was equivalent to an increase

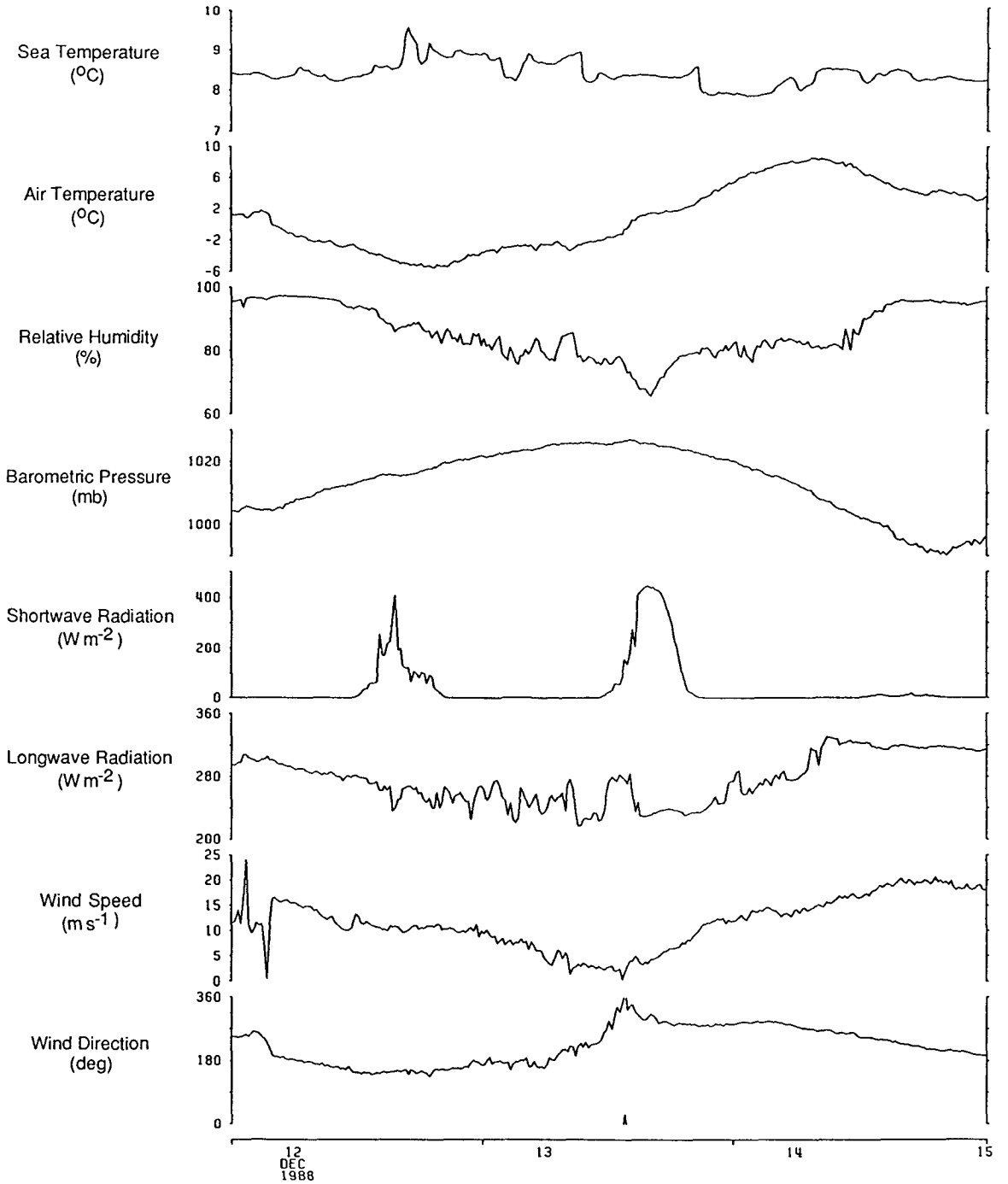

FIG. 5. Meteorological data measured during IOP 2 from V-161WR. From top to bottom: Sea surface temperature (°C), air temperature (°C), relative humidity (%), barometric pressure (mb), incident solar radiation (W m^{-2}), downward longwave radiation (W m^{-2}), wind speed (m s^{-1}), and wind direction (°). Note that the wind direction is in oceanographic coordinates. The value represents the direction to which the wind is blowing.

of the sky temperature from −8° to 7°C, which was an indication of the arrival of lower and warmer clouds. The rapid passage of a warm front was observed at the buoy at 0500 UTC as the winds quickly veered by 130° from the east to from the southwest in 30 min. For about six hours, the buoy was in the warm air ahead of the approaching cold front as the air temperature remained fairly constant at about 7°C. The relative

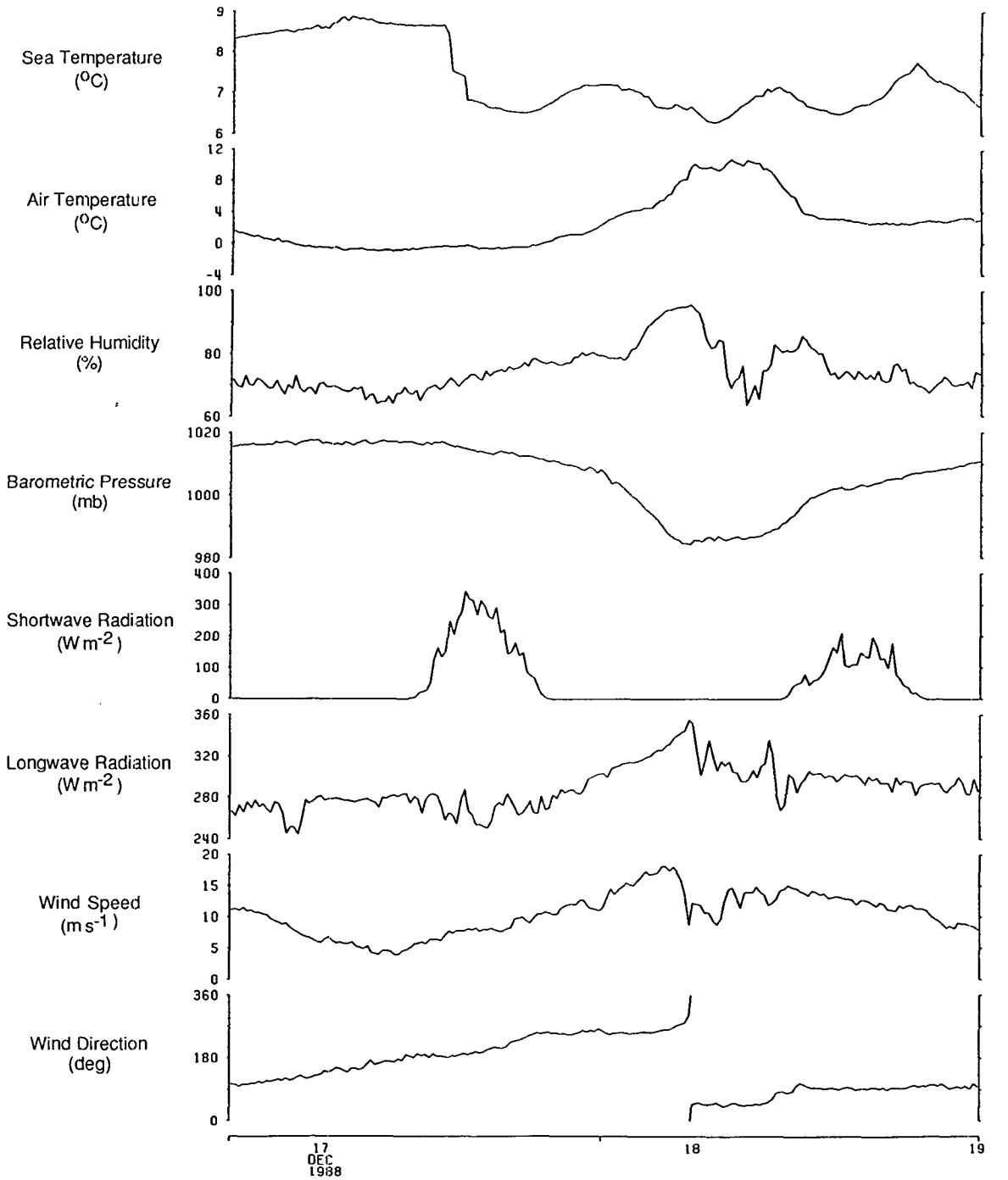

FIG. 6. Same as Fig. 5 for IOP 3.

humidity, longwave radiation, and wind speed displayed some variability during this time. The passage of a cold front was observed just prior to 1200 UTC in which the winds veered from the southwest to from the west over the course of about one hour. The sea surface temperature remained relatively unchanged; however, the air temperature quickly dropped to about 4°C as cold air moved into the area. Gradual decreases in the relative humidity, wind speed, and longwave radiation were noted as the storm moved away from the buoy. However, the region was dominated by cloudy conditions on 18 December when the maxi-

mum incident solar radiation values reached only to 200 W m^{-2}. Again, this observation was supported by GOES imagery (Hartnett and Browne 1989).

c. IOP 4

This storm started out as twin cyclones that were triggered by two strong upper-level disturbances. The second storm (the storm that IOP 4 was dedicated to) may have been the deepest observed extratropical cyclone south of 40°N in the North Atlantic Ocean this century (Hartnett et al. 1989). The central surface barometric pressure was estimated between 938 and 940 mb with winds approaching 45 m s^{-1} during the mature stage of the storm. The storm path was much like that in IOP 2 except 150 km closer to the buoy (Fig. 4c). A barometric pressure drop of 26 mb in 17 h was observed at the buoy on 4 January (Fig. 7) as the storm center came within 300 km of the mooring. The minimum observed pressure at the buoy was 971 mb at 2200 UTC on that same day. A pressure gradient of 10 mb (100 km)$^{-1}$ was estimated between the storm center and buoy at 0000 UTC on 5 January.

A warm-core ocean eddy had moved into the region, resulting in an anomalously warm sea surface temperature of 14°C. The warm sea temperature was also observed at 20 m by the VMCM. The sea surface temperature remained at 14°C until the storm moved away from the area. The sea surface temperature then dropped to 3°C in 24 h as the eddy continued its transit across the area. The air temperature dropped as cold continental air was swept in behind the storm. The temperature had been about 6°C before the approach of the storm and dropped to −2°C after its passage. The relative humidity during IOP 4 was generally high and remained near saturation. The solar irradiance was quite low for 3, 4, and 5 January as this storm was associated with a substantial cloud cover (Hartnett and Browne 1989). The incident solar irradiance never exceeded 50 W m^{-2} on 4 January. The downward longwave flux was generally high, averaging about 300 W m^{-2} (equivalent sky temperature of about −3°C). Wind speeds were also high, reaching up to 20 m s^{-1}, for 12 h during the closest approach of the storm. The wind direction veered from the northwest to from the northeast as the storm approached and eventually backed to from the northwest as the storm moved away from the area.

4. Air–sea heat fluxes

Estimates of the total surface heat flux were computed from the data using

$$Q_T = Q_S + Q_L + Q_H + Q_E \qquad (4.1)$$

where Q_T is the total heat flux, Q_S is the net solar irradiance, Q_L is the net longwave radiation flux, Q_H is the sensible heat flux, and Q_E is the latent heat flux. Each component of the total heat flux is positive when the heat flows from the ocean into the atmosphere. The net solar irradiance at the sea surface was determined by

$$Q_S = -(1 - \alpha)\mathrm{SW} \qquad (4.2)$$

where SW is the measured downward solar radiation (W m^{-2}), and α is the albedo of the sea surface (0.06). The net longwave irradiance at the sea surface was determined using

$$Q_L = \epsilon\sigma(T_S + 273.15)^4 - \mathrm{LW} \qquad (4.3)$$

where LW is the observed downward longwave radiation (W m^{-2}), T_S is the sea surface temperature (°C), ϵ the emissivity of the sea surface (0.97), and σ is the Stefan–Boltzman constant (5.67×10^{-8} W m^{-2} K^{-4}). The sensible (Q_H) and latent (Q_E) heat fluxes were computed from bulk aerodynamic formulas (Large and Pond 1982) and are estimated by

$$Q_H = \rho C_p C_H (T_S - T_A) U$$

$$Q_E = \rho L_v C_E (q_S - q_A) U$$

where ρ is the density of the air, C_p is the specific heat of dry air, L_v is the latent heat of vaporization, C_H is the transfer coefficient for sensible heat (Stanton number), C_E is the transfer coefficient for latent heat (Dalton number), T_S and T_A are the sea surface temperature and air temperature, respectively, q_S and q_A are the saturation specific humidity and specific humidity, respectively, and U is the wind speed.

As seen in the previous section, the buoy was located in a region where rapid changes in the surface meteorology were commonplace. The bulk formulas have limitations and uncertainties in such an environment. As stated by Large and Pond (1982), the exchange coefficients are suspect in a rapidly changing wind field. In addition, the direction of the wind stress may not be the same direction as the wind velocity if the wave field is changing or has complex directionality. However, for long-term observations over the ocean from a surface buoy, the bulk formula method still remains the only practical technique for estimating surface fluxes of heat, moisture, and momentum. The propagation of measurement error, independent of the uncertainty in the transfer coefficients, through the bulk formulas has been described by Weller et al. (1990). Since the measurement errors found in the ERICA data are comparable to those found by Weller et al., we can use the same uncertainties here in this study. The uncertainty of the net solar and longwave radiation fluxes lies from 5 to 15 W m^{-2}. The sensible heat flux has an uncertainty of 1.5–3 W m^{-2}, while the latent heat flux is accurate to within 20 W m^{-2}.

The monthly and total deployment estimates of the surface-layer heat fluxes are given in Table 3. The

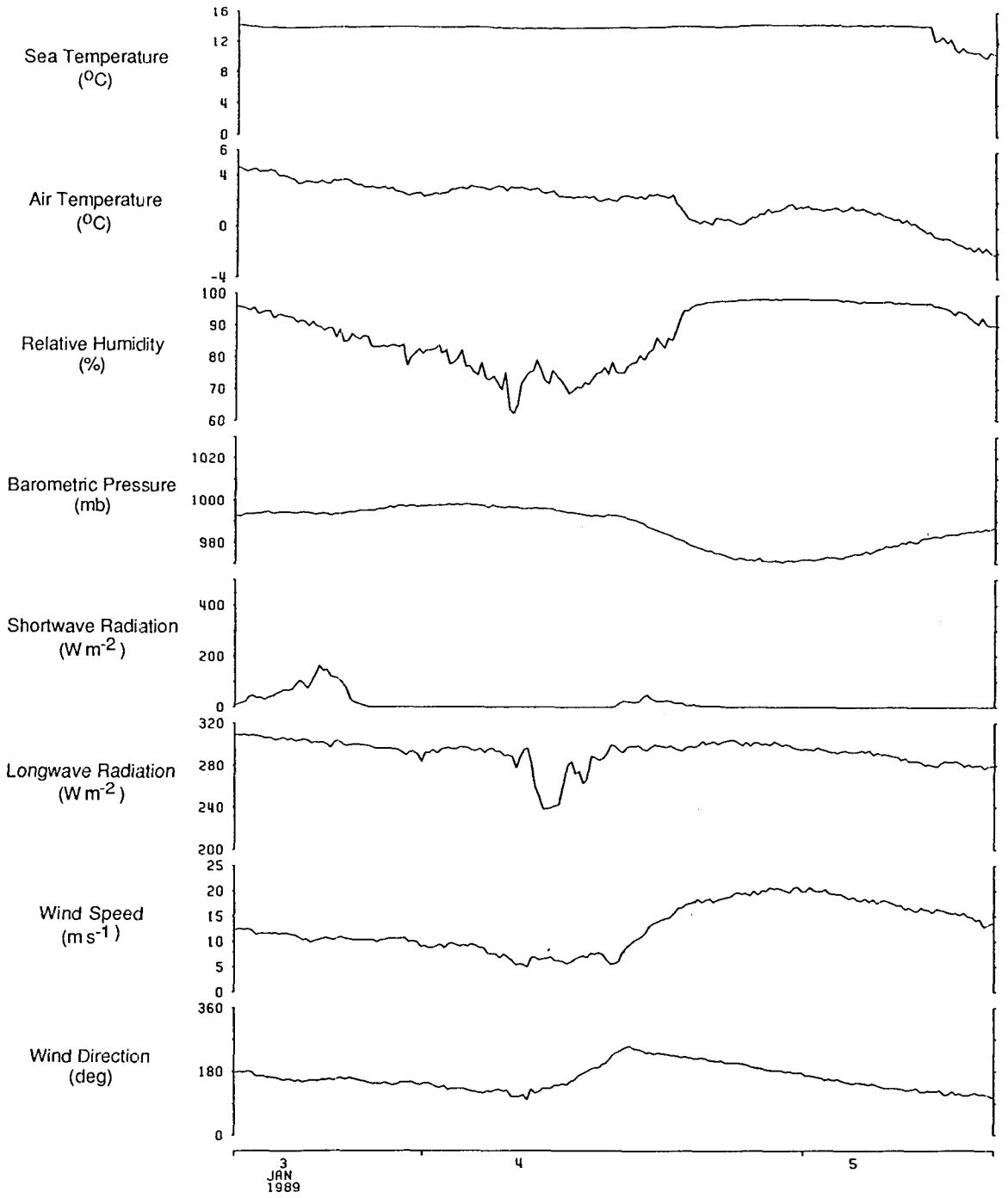

FIG. 7. Same as Fig. 5 for IOP 4.

monthly mean net shortwave radiation was the only component of the total heat flux that contributed to oceanic heating. This heating dropped to a minimum during December and January, in part due to a lower solar angle and overall increased cloudiness (Isemer and Hasse 1985). The monthly mean net longwave flux was positive and did not change significantly over the five-month period. These monthly averaged net radiation fluxes were in good agreement with climatological values for the same area of the North Atlantic Ocean (Isemer and Hasse 1987). The sensible and latent heat fluxes were largest during November and De-

TABLE 3. Estimates of the monthly and total deployment mean air–sea fluxes at the ERICA mooring.

	October*	November	December	January	February	Total**
Q_S (W m^{-2})	−91.1	−62.2	−44.2	−43.7	−74.5	−61.2
Q_L (W m^{-2})	47.0	56.1	53.5	41.2	37.4	47.1
Q_H (W m^{-2})	19.0	69.3	71.2	55.1	24.1	51.1
Q_E (W m^{-2})	79.7	149.6	94.8	63.8	21.3	81.3
Q_T (W m^{-2})	54.7	212.8	175.3	116.4	8.2	118.2
τ_x (N m^{-2})	−0.004	0.145	0.065	0.055	0.038	0.069
τ_y (N m^{-2})	0.003	−0.039	−0.064	−0.083	−0.012	−0.045

* 18 October–31 October 1988
** 18 October 1988–6 March 1989

cember when the air–sea temperature differences were relatively large. The latent heat flux was four times larger than the sensible heat flux in late October but dropped to only two times as large in November. During the remaining three months the magnitudes of these two fluxes were comparable. Both fluxes decreased dramatically during January and February. These fluxes were also in fair agreement with those determined by Bunker (Isemer and Hasse 1987). The overall total heat flux for the deployment showed a net cooling of the ocean or net warming of the atmosphere with the largest contribution during November. During November and December, the sensible and latent heat fluxes contributed significantly to heating the atmosphere. However, by February, they contributed little as the net short- and longwave radiation fluxes dominated the surface energy transfer.

The mean estimates of the surface fluxes for the three IOP case-study events are given in Table 4 and are discussed next.

a. IOP 2

The average surface heat flux for IOP 2 was estimated at about 300 W m^{-2} (Fig. 8). The total heat flux was about 600–700 W m^{-2} during the cold-air outbreak preceding the bomb. As the storm approached the total heat flux dropped to nearly zero and reversed sign for a short time. During the storm's closest approach the total heat flux ranged from 200 to 300 W m^{-2}. The average net solar irradiance for IOP 2 was −44 W m^{-2}. This was the only component of the total heat flux that contributed to the warming of the oceanic surface layer. Almost no solar radiation was received at the surface on 14 December. The average net longwave radiation for IOP 2 was 74 W m^{-2}. Before the storm, the flux ranged from 100 to 130 W m^{-2}. As the lower and warmer clouds moved over the buoy, the net longwave flux dropped to about 30 W m^{-2}.

TABLE 4. Mean estimates of the upward surface-layer fluxes at the ERICA mooring during IOPs 2, 3, and 4.

	IOP 2	IOP 3	IOP 4
Q_S (W m^{-2})	−44.3	−44.5	−13.3
Q_L (W m^{-2})	73.7	51.1	79.8
Q_H (W m^{-2})	126.7	85.4	299.5
Q_E (W m^{-2})	141.7	122.1	361.7
Q_T (W m^{-2})	297.9	214.0	727.7
τ_x (N m^{-2})	−0.267	0.028	0.101
τ_y (N m^{-2})	−0.213	−0.036	−0.433

The biggest contributing components were the sensible and latent heat fluxes. The average sensible and latent heat fluxes for the IOP were 127 and 142 W m^{-2}, respectively. These estimates were approximately one-and-a-half to two times larger than the monthly climatological means of 71 and 95 W m^{-2} (Isemer and Hasse 1987). Both of these fluxes were fairly large in the cold air that preceded the storm. The sensible heat flux was about 300 W m^{-2} while the latent heat flux was about 250 W m^{-2}. However, as warmer air was advected into the region, these fluxes dropped down to 0 and 100 W m^{-2}, respectively. As the storm passed and moved out of the area, these fluxes increased again at the arrival of more cold air.

A very simple budget between the heat transfer at the air–sea interface and the change in upper-ocean heat content was examined. The total heat transfer from the ocean to the atmosphere was computed using

$$H_{\text{surf}} = \int Q_T dt \tag{4.4}$$

where dt is the time interval between measurements (900 s). For IOP 2, the integrated heat transfer was 0.61×10^8 J m^{-2} (Table 5). Because only one mooring with two current meters was deployed a complete determination of the oceanic component of the heat budget was not possible. Vertical and horizontal advection and mixing could not be estimated. However, using the sea surface temperature and the sea temperature at 20 m, the average heat content for the upper 20 m of the ocean was computed using

$$H_{\text{sea}} = \rho C_p z \bar{T} \tag{4.5}$$

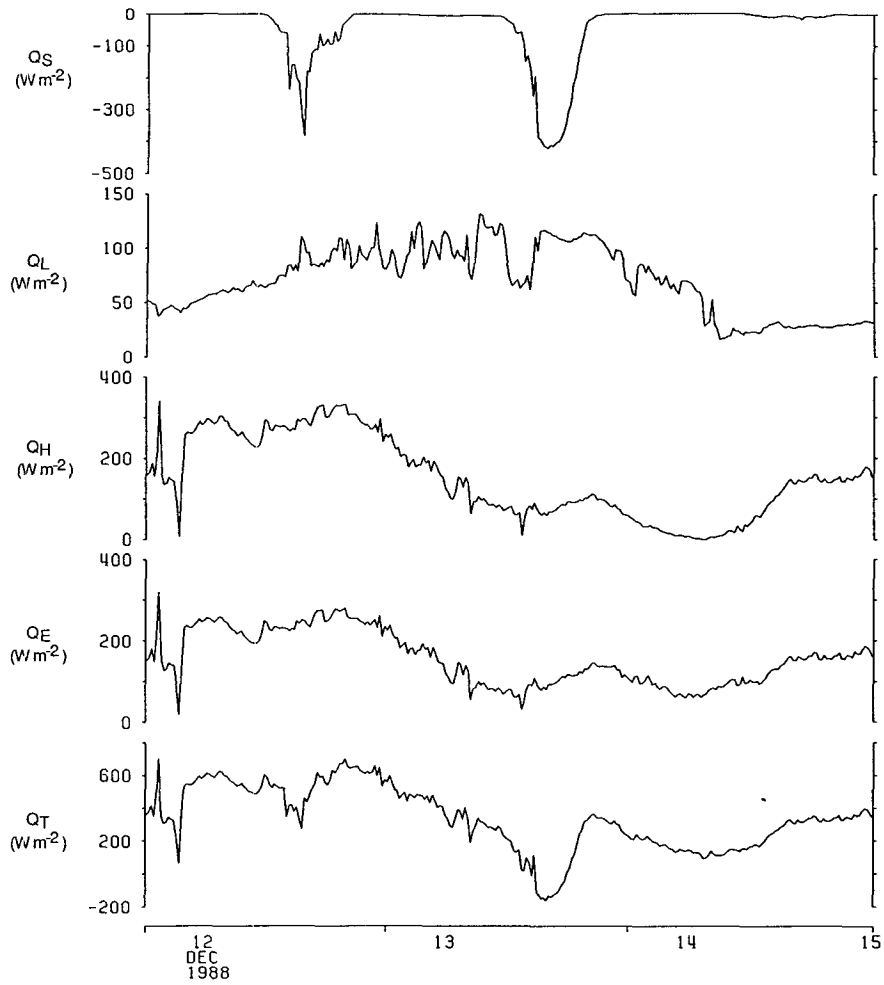

FIG. 8. Surface-layer heat flux estimates (W m^{-2}) during IOP 2. From top to bottom: Net surface solar irradiance Q_S net longwave radiation flux Q_L, sensible heat flux Q_H, latent heat flux Q_E, and total heat flux Q_T.

where ρ is the density of sea water (1024 kg m^{-3}), C_p is the specific heat at constant pressure of sea water (4183 J kg^{-1} K^{-1}), z is the thickness of the layer (20 m), and $\bar{T}$ is the mean sea temperature of the layer. For IOP 2, the average heat content was 7.27×10^8 J m^{-2}. The change in the ocean heat content was -0.58×10^8 J m^{-2}, which is equivalent to a decrease in sea temperature of 0.7°C. In this case, the heat lost by the upper 20 m is nearly equivalent to that put into the atmosphere at the air–sea interface. While it may be possible for this bomb to rob the upper ocean of its heat, no assumptions are made in this budget about the advection of warmer or cooler water. During IOP 2, the mean current velocity at 20 m was from the east at 17.8 cm s^{-1}.

TABLE 5. Total surface energy transfer and upper 20-m ocean heat content during IOPs 2, 3, and 4.

IOP	H_{surf} ($\times 10^8$ J m^{-2})	H_{sea} ($\times 10^8$ J m^{-2})	ΔH_{sea} ($\times 10^8$ J m^{-2})
2	0.61	7.27	−0.58
3	0.37	6.39	−1.44
4	1.26	11.74	−2.52

b. IOP 3

Like the previous IOP, the total heat flux was large during the cold-air outbreak preceding the storm but dropped to nearly zero during the storm (Fig. 9). The average total heat flux for IOP 3 was 214 W m^{-2}. The total heat flux was about 400 W m^{-2} in the cold air preceding the storm. When the warm front passed through the area, the total heat flux switched signs and was approximately −100 W m^{-2}. When the cold front

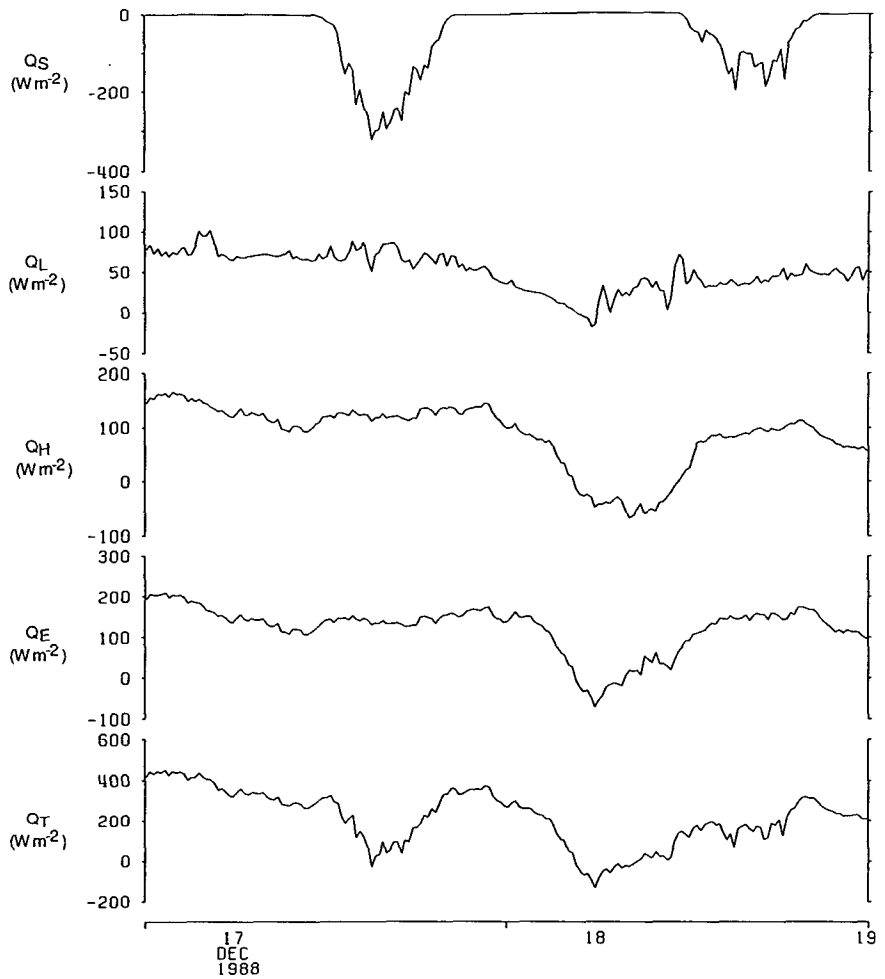

FIG. 9. Same as Fig. 8 for IOP 3.

passed several hours later, the total heat flux was again positive and increased to over 200 W m^{-2}.

The net solar and longwave fluxes nearly offset each other with average values for IOP 3 of −45 and 51 W m^{-2}. The net longwave flux ranged from 0 to 100 W m^{-2}, with the lowest values occurring just prior to the passage of the warm front. The average sensible and latent heat fluxes for IOP 3 were 85 and 122 W m^{-2}, respectively. The temporal variability of the two fluxes was similar, much like that seen in IOP 2. The sensible heat flux was about 150 W m^{-2} during the cold-air outbreak preceding the storm. The flux then reversed in the warm-air region with typical values of about −50 W m^{-2}. As the cold front passed, the sensible heat flux became positive again and rose to about 100 W m^{-2}. The latent heat flux went through a similar sequence starting at 200 W m^{-2}, dropping to nearly −100 W m^{-2}, and then rising up to about 200 W m^{-2}.

The total air–sea heat transfer during IOP 3 was 0.37 × 10^8 J m^{-2}. The mean heat content was 6.39 × 10^8 J m^{-2} with a change of −1.44 × 10^8 J m^{-2}, or a drop in sea temperature of 1.7°C. In this case, the drop of upper-ocean heat content greatly exceeds the heat given up to the atmosphere. This might suggest that advective fluxes of colder waters would account for a drop in the sea temperature. That is possible since the mean current velocity at 20 m was from the northeast at 27.1 cm s^{-1}.

c. *IOP 4*

Strong winds and a large air–sea temperature difference of up to 12°C created large heat fluxes during IOP 4 (Fig. 10). The average total heat flux for the 48-h period was 728 W m^{-2}. This was nearly two to three times the total heat flux observed in IOP 2 or 3. However, it must be pointed out again that a warm-core eddy passing through the mooring was responsible for the anomalously large surface heat fluxes. During the most intense part of the storm, the total heat flux approached 1200 W m^{-2}; and a total heat flux of at least 1000 W m^{-2} was sustained for 15 h during this time.

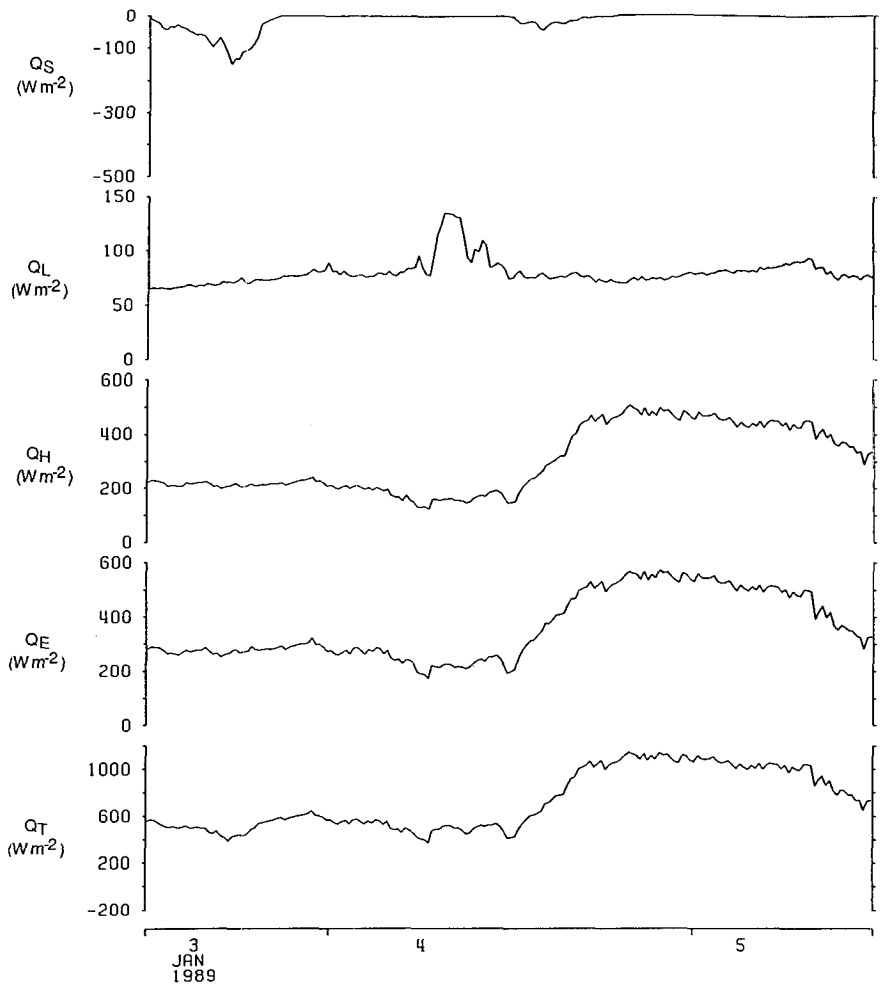

FIG. 10. Same as Fig. 8 for IOP 4.

As the storm quickly moved away from the area, however, the total heat fluxes dropped.

Satellite imagery depicted substantial cloud cover over much of the western North Atlantic Ocean from this bomb (Hartnett and Browne 1989). As a result, the net solar irradiance contribution to the total heat flux was small to negligible. The mean flux was only -13 W m^{-2} for IOP 4. On 4 January, the net solar irradiance never exceeded -50 W m^{-2}. The average net longwave flux was larger in this event with a value of 80 W m^{-2}. The typical range was between 50 and 150 W m^{-2}. The largest contributors to the total heat flux were the sensible and latent heat fluxes. Mean estimates for IOP 2 were 300 and 362 W m^{-2}, respectively. The sensible heat flux reached 500 W m^{-2}, while the latent heat flux was nearly 570 W m^{-2} during the storm's closest approach.

The integrated air–sea heat exchange was large in this storm, with an estimated value of 1.26×10^8 J m^{-2}. The total heat content of the upper ocean was also quite substantial at 11.74×10^8 J m^{-2}. The change in heat content was -2.52×10^8 J m^{-2}, which is equivalent to a drop in temperature of -2.9°C. However, advective processes are clearly the dominant factor in this particular case as the warm-core eddy had made its transit past the mooring coincident with IOP 4.

5. Air–sea momentum fluxes

In addition to examining the heat transfer at the air–sea interface, the momentum transfer was studied. East and north surface stresses were also computed from bulk aerodynamic formula fluxes (Large and Pond 1981). The stress was estimated by

$$\tau_x = \rho C_D u |u|$$

$$\tau_y = \rho C_D v |v|$$

where ρ is the density of air, C_D is the drag coefficient, and u and v are the eastward and northward wind ve-

locity, respectively. The monthly averages are listed in Table 3. During the last two weeks of October, the average surface stress was weak and from the southeast. This was due to the high variability of the wind velocity. However, that quickly changed for the next three months as a strong flow from the northwest dominated the mooring area. This was typical of the strong cold-air outbreaks over the western North Atlantic Ocean coming from Canada. By February, the mean stress values had decreased. These monthly estimates are in reasonable agreement with those determined by Bunker (Isemer and Hasse 1987).

The stress estimates were typically quite large during many of these winter storms. The mean stress estimates for IOPs 2, 3, and 4 are listed in Table 4. The average east and north stress for IOP 2 was -0.267 N m^{-2} and -0.213 N m^{-2}, respectively. The stress direction was from the northeast. Near the end of IOP 2, the surface stress reached up to 1.4 N m^{-2}. For IOP 3, the mean east and north stress was 0.028 and -0.036 N m^{-2}. These mean values were small since the wind velocity had rotated a full 360° over the 48-h period. In some instances, the total surface stress reached 1.0 N m^{-2}. In IOP 4, the mean east and north components of stress were 0.101 and -0.433 N m^{-2}. Individual observations reached magnitudes of up to 1.4 N m^{-2}.

To further understand how the surface stresses and upper ocean were interrelated, rotary autospectra were computed. This was done to examine the variability over a range of frequencies. Positive frequencies corresponded to vectors that rotated counterclockwise with time. Conversely, negative frequencies corresponded to clockwise-rotating vectors. The autospectra of the surface stress is shown in Fig. 11a. The positive and negative frequencies both displayed similar behavior with most of the variability in the frequencies below 0.02 h^{-1}. This corresponded to periods greater than 2 days. Two peaks were found in the autospectra of the 20-m current velocity (Fig. 11b). The largest peak was found at 0.05–0.06 h^{-1} for the clockwise (negative fre-

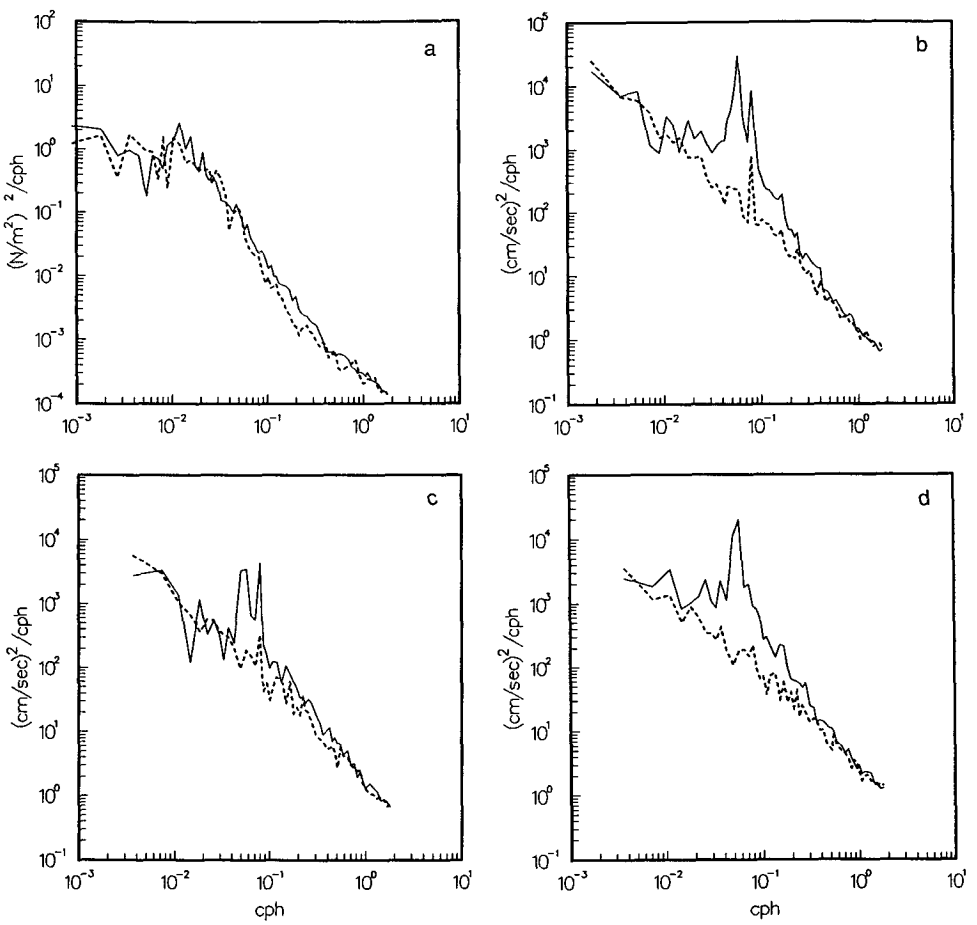

FIG. 11. Autospectra of (a) surface stress, (b) 20-m current velocity, (c) 50-m current velocity, and (d) current velocity difference between 20 and 50 m. The solid line represents the clockwise (negative frequency) rotating velocity vector. The dashed line represents the counterclockwise (positive frequency) rotating velocity vector.

quency) rotating velocity vector. This peak was associated with oscillatory flow at the inertial period of 17.8 h [$12/\sin(\phi)$, where ϕ is the latitude]. The second peak was found in both positive and negative frequencies at about 0.08 h^{-1}. This peak corresponded to the semidiurnal tidal flow with a period of about 12 h. Similar spectral peaks were found in the spectra of the 50-m current velocity (Fig. 11c). The autospectra of the difference or shear between the 20- and 50-m velocity showed a peak corresponding to the inertial period only (Fig. 11d).

Coherence between the surface stress and ocean currents was also constructed. The stress and 20-m current velocity (Fig. 12a) were highly coherent for the clockwise-rotating velocity vectors in the subinertial frequencies. The same was true for the counterclockwise-rotating velocity vectors; however, the coherence estimates at the subinertial frequencies were much smaller. The phase angle for these same frequencies was about 90°. Physically, this information tells us that the low-frequency ocean current in the upper 20 m was moving perpendicular to and to the right of the surface wind. There was very little coherence between the two time series for periods less than 24 h in both positive and negative frequencies.

The same coherence and phase plots were created between the surface stress and 50-m current velocity (Fig. 12b). However, in this case, the surface stress and 50-m current velocity were only weakly coherent in the subinertial frequencies for both clockwise- and counterclockwise-rotating vectors. Very little coherence was evident in the higher frequencies. This would suggest that the surface forcing by the wind had only small effects on the current at 50 m. This was also supported by the coherence plot of the surface stress and 20- and 50-m difference velocity (Fig. 12c). The clockwise-rotating vectors are coherent at the subinertial frequencies. This would suggest that the upper 20 m responded to atmospheric forcing and acted somewhat independently of the ocean at 50 m.

This atmospheric forcing can be visualized by the use of a progressive vector diagram (Fig. 13). The vector displacements associated with the vector velocity difference between the two current meters was plotted

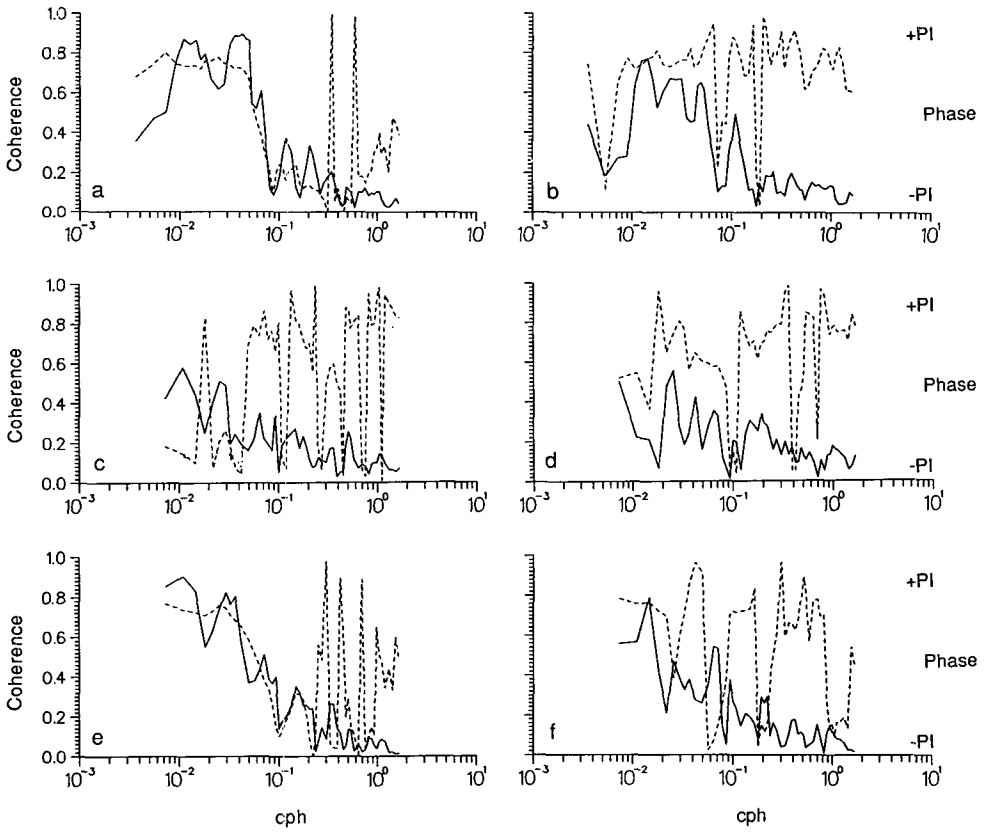

FIG. 12. Coherence (solid line) and phase (dashed line) between (a) surface stress and clockwise-rotating velocity vector at 20 m, (b) surface stress and counterclockwise-rotating velocity vector at 20 m, (c) surface stress and clockwise-rotating velocity vector at 50 m, (d) surface stress and counterclockwise-rotating velocity vector at 50 m, (e) surface stress and clockwise-rotating vector of difference between 20 and 50 m, and (f) surface stress and counterclockwise-rotating velocity vector of difference between 20 and 50 m.

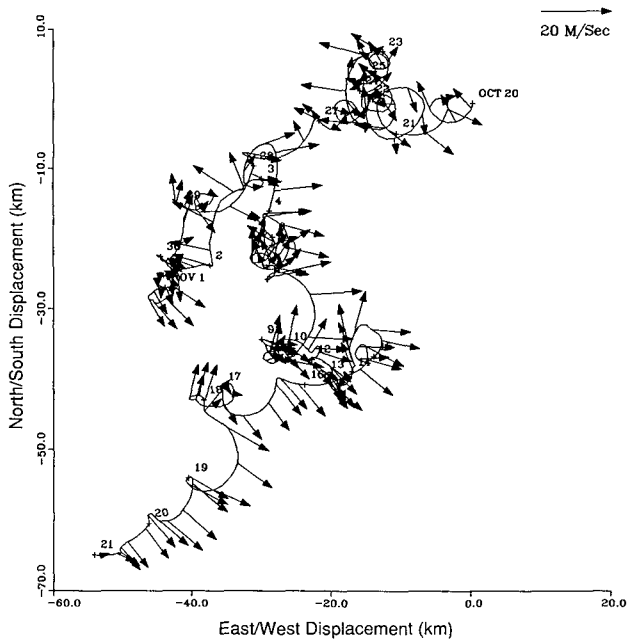

FIG. 13. Progressive vector diagram of the difference velocity between 20 and 50 m from 20 October to 21 November. Four-hour-average wind vectors are superimposed to show the forcing of the upper ocean by the surface wind.

with the mean wind vectors superimposed. For the first several days of the deployment (Fig. 14), the upper ocean responded with classic inertial oscillations and a slight movement toward the west. The atmospheric forcing during these first few days was somewhat variable. Recall that the mean surface stress components were nearly zero for the last two weeks of October. However, as the winds blew more consistently from the northwest in November, the upper ocean responded by moving to the right of the mean wind toward the southwest. This was very apparent from 13 to 20 November as the 20-m current velocity showed a displacement of 50 km relative to the 50-m current velocity. The mean velocity of that transit was computed at approximately 8 cm s^{-1}. Unfortunately, no further estimates could be made since the 50-m current data were lost in late November.

Strong and persistent westerly and northwesterly winds coming off the North American continent were the dominant weather feature of November, December, and January. We can infer that this type of atmospheric forcing would transport cold water toward the south. Inevitably, colder water either from below or from the north must replace the transported water. If this was the case, then the primary reason for the cooling of the upper ocean was principally due to wind forcing.

6. Summary and conclusions

A mooring was deployed about 300 km southeast of Nova Scotia during ERICA in an attempt to obtain high-quality meteorological and near-surface oceanographic measurements of rapidly intensifying cyclones. Complete high-resolution time series of sea surface temperature, air temperature, relative humidity, barometric pressure, incident solar radiation, downward longwave radiation, and wind velocity were acquired. A limited time series of oceanographic current and temperature data were acquired at 20 and 50 m beneath the sea surface.

Three case studies were presented where rapidly intensifying cyclones approached and passed by the mooring. The surface meteorology of each storm was described in detail. Estimates of the net solar, net longwave, sensible, and latent heat flux were computed from bulk aerodynamic formulas for each storm. The total surface heat flux was generally quite large during the cold-air outbreaks preceding and following these storms. The total surface heat flux approached 1200 W m^{-2} for a short time during one such storm. While the surface heat fluxes may sometimes reduce the heat content of the upper-ocean water, our limited study of the change of the total heat content in the upper 20 m suggests that at this location change in ocean surface temperature is governed by advective processes within the ocean.

An examination of the momentum transfer at the air–sea interface showed that the upper 20-m ocean layer was forced by the atmospheric winds. Although the current-meter data were prematurely cut short, we may speculate that persistent west and northwest winds

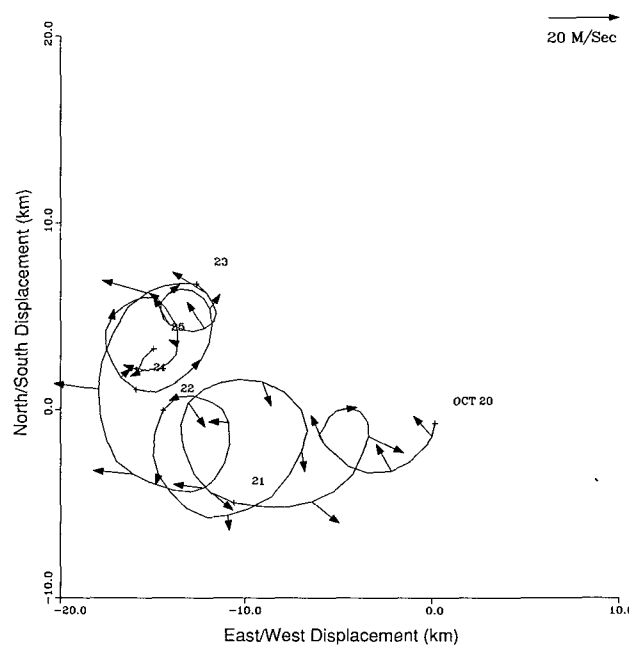

FIG. 14. Enlargement of progressive vector diagram from 20 to 25 October to show the inertial oscillatory behavior of the upper ocean.

off the North American continent may have been sufficient to force the warm waters south, thereby being the mechanism responsible for oceanic cooling.

The next logical step in examining the air–sea flux contribution to these storms would be to combine this dataset with other nearby surface observations. A detailed spatial distribution of the surface-layer fluxes may be constructed, especially in the areas near the Gulf Stream where large air–sea temperature differences may exist. This dataset may also be valuable as a ground-truth reference of remotely sensed data. The same is true when used as a surface reference point in the examination of the vertical distribution of the sensible and latent heat fluxes obtained from aircraft profiles and dropsondes. In short, there are many more opportunities to exploit this dataset to further our understanding of how the marine atmospheric boundary layer and upper ocean behave in the vicinity of rapidly intensifying cyclones.

Acknowledgments. The authors would like to thank Susan Tarbell for her help with the data processing from start to finish, Nancy Pennington for her help in data analysis and preparation of many of the figures, and Mary Ann Lucas for preparation of the manuscript. Thanks to the numerous individuals involved with the development, construction, deployment, and retrieval of the mooring used in ERICA. This work was funded by the Office of Naval Research under Contract N00014-84-C-0134, NR 083-400, and Grant N00014-90J-1423 and is Contribution Number 7779 from the Woods Hole Oceanographic Institution. This research was partially funded by the Texas Institute of Oceanography, the Institute for Naval Oceanography, the National Weather Service–Southern Region, and Texas A&M University, through the Cooperative Institute for Applied Meteorological Studies.

REFERENCES

Crescenti, G. H., S. A. Tarbell, and R. A. Weller, 1991: A compilation of moored current meter data and wind recorder data from the severe environment surface mooring (SESMOOR) Volume XLIII. Tech. Rep., WHOI-91-18, 49 pp. [Woods Hole Oceanogr. Inst., Woods Hole, MA 02543.]

Davis, C. A., and K. A. Emanuel, 1988: Observational evidence for the influence of surface heat fluxes on rapid maritime cyclogenesis. *Mon. Wea. Rev.*, **116,** 2649–2659.

Dean, J. P., and R. C. Beardsley, 1988: A vector-averaging wind recorder (VAWR) system for surface meteorological measurements in CODE (Coastal Ocean Dynamics Experiment). Tech. Rep., WHOI Ref. 88-20, 74 pp. [Woods Hole Oceanogr. Inst., Woods Hole, MA 02543.]

Hadlock, R., and C. W. Kreitzberg, 1988: The Experiment on Rapidly Intensifying Cyclones over the Atlantic (ERICA) field study: Objective and plans. *Bull. Amer. Meteor. Soc.*, **69,** 1309–1320.

Hartnett, E., and C. Browne, 1989: *Experiment on Rapidly Intensifying Cyclones over the Atlantic Satellite Atlas.* Drexel University, 226 pp.

——, G. Forbes, and R. Hadlock, 1989: Experiment on Rapidly Intensifying Cyclones over the Atlantic field phase summary. Battelle Ocean Sciences, Richland, Washington.

Isemer, H.-J., and L. Hasse, 1985: *The Bunker Climate Atlas of the North Atlantic Ocean. Volume 1: Observations.* Springer-Verlag, 218 pp.

——, and ——, 1987: *The Bunker Climate Atlas of the North Atlantic Ocean. Volume 2: Air–Sea Interactions.* Springer-Verlag, 252 pp.

Kery, S. M., 1989: Severe environment surface mooring (SESMOOR). *Oceans '89, IEEE,* Seattle, Washington, 1398–1405.

Large, W. G., and S. Pond, 1981: Open ocean momentum flux measurements in moderate to strong winds. *J. Phys. Oceanogr.*, **11,** 324–336.

——, and ——, 1982: Sensible and latent heat flux measurements over the ocean. *J. Phys. Oceanogr.*, **12,** 464–482.

Marine Weather Review, North Atlantic Ocean, 1989: *Mariners Weather Log,* **33,** 40–46.

Nuss, W. A., and R. A. Anthes, 1987: A numerical investigation of low-level processes in rapid cyclogenesis. *Mon. Wea. Rev.*, **115,** 2728–2743.

Payne, R. E., 1974: A buoy-mounted meteorological recording package. Tech. Rep., WHOI Ref. 74-40, 32 pp. [Woods Hole Oceanogr. Inst., Woods Hole, MA 02543.]

Pyke, C. E., 1965: On the role of air–sea interaction in the development of cyclones. *Bull. Amer. Meteor. Soc.*, **46,** 4–15.

Reed, R. J., and W. Blier, 1986a: A case study of comma cloud development in the eastern Pacific. *Mon. Wea. Rev.*, **114,** 1681–1695.

——, and ——, 1986b: A further study of comma cloud development in the eastern Pacific. *Mon. Wea. Rev.*, **114,** 1696–1708.

Roebber, P. J., 1984: Statistical analysis and updated climatology of explosive cyclones. *Mon. Wea. Rev.*, **112,** 1577–1589.

Sanders, F., and E. P. Auciello, 1989: Skill in prediction of explosive cyclogenesis over the western North Atlantic Ocean, 1987/88: A forecast checklist and NMC dynamical models. *Wea. Forecasting,* **4,** 157–172.

——, and J. R. Gyakum, 1980: Synoptic–dynamic climatology of the "bomb." *Mon. Wea. Rev.*, **108,** 1589–1606.

Wash, C. H., J. E. Peak, W. E. Calland, and W. A. Cook, 1988: Diagnostic study of explosive cyclogenesis during FGGE. *Mon. Wea. Rev.*, **116,** 431–451.

Weller, R. A., and R. E. Davis, 1980: A vector measuring current meter. *Deep-Sea Res.*, **27A,** 565–582.

——, D. L. Rudnick, R. E. Payne, J. P. Dean, N. J. Pennington, and R. P. Trask, 1990: Measuring near-surface meteorology over the ocean from an array of surface moorings in the subtropical convergence zone. *J. Atmos. Oceanic Technol.*, **7,** 85–103.

Winston, J. S., 1955: Physical aspects of rapid cyclogenesis in the Gulf of Alaska. *Tellus,* **7,** 481–500.